Chapter 18

An Introduction to Magnetic Tweezers

David Dulin

Abstract

Magnetic tweezers are a single-molecule force and torque spectroscopy technique that enable the mechanical interrogation in vitro of biomolecules, such as nucleic acids and proteins. They use a magnetic field originating from either permanent magnets or electromagnets to attract a magnetic particle, thus stretching the tethering biomolecule. They nicely complement other force spectroscopy techniques such as optical tweezers and atomic force microscopy (AFM) as they operate as a very stable force clamp, enabling long-duration experiments over a very broad range of forces spanning from 10 fN to 1 nN, with 1–10 milliseconds time and sub-nanometer spatial resolution. Their simplicity, robustness, and versatility have made magnetic tweezers a key technique within the field of single-molecule biophysics, being broadly applied to study the mechanical properties of, e.g., nucleic acids, genome processing molecular motors, protein folding, and nucleoprotein filaments. Furthermore, magnetic tweezers allow for high-throughput single-molecule measurements by tracking hundreds of biomolecules simultaneously both in real-time and at high spatiotemporal resolution. Magnetic tweezers naturally combine with surface-based fluorescence spectroscopy techniques, such as total internal reflection fluorescence microscopy, enabling correlative fluorescence and force/torque spectroscopy on biomolecules. This chapter presents an introduction to magnetic tweezers including a description of the hardware, the theory behind force calibration, its spatiotemporal resolution, combining it with other techniques, and a (non-exhaustive) overview of biological applications.

Key words Single-molecule biophysics, Magnetic tweezers, Force spectroscopy, Protein-nucleic acids interactions, Torque spectroscopy

1 Brief History and Application of Magnetic Tweezers

Magnetic tweezers use the magnetic field generated by permanent or electromagnets to apply force and/or rotate magnetic particles attached to a biological material, hence inducing a mechanical stress. The first biophysics assay using a magnetic actuator in a biological context was reported by Crick and Hughes in 1950 [1], where magnetic particles placed in the cytoplasm of a cell were displaced to interrogate its viscoelastic properties. Magnetic tweezers have two main areas of application in biophysics: cellular mechanics and single-molecule biophysics. The force applied in

Iddo Heller et al. (eds.), *Single Molecule Analysis: Methods and Protocols*, Methods in Molecular Biology, vol. 2694,
https://doi.org/10.1007/978-1-0716-3377-9_18,

cellular mechanics is usually relatively large (≫ 1 nN) [2, 3] compared to the single-molecule world (≪100 pN) [4], and therefore their respective instrument designs differ significantly. Here, we solely focus on magnetic tweezers assays for single-molecule biophysics.

In the 1990s, the Bustamante lab and the Croquette and Bensimon lab pioneered the modern version of single-molecule magnetic tweezers capable of applying a constant force (even below 1 pN) and torque, enabling the interrogation of DNA mechanical properties at the single-molecule level [5, 6]. Nowadays, magnetic tweezers are found in many labs around the world, and single-molecule studies have been performed on various protein-nucleic acids systems [7], ranging from helicases [8] to DNA polymerases [7–9], topoisomerases and gyrases [10–13], cellular and viral RNA polymerases [14], nucleoprotein filaments [15–18], and the mechanical stability of protein folding and protein-ligand interactions [19–23]. The simplicity and the robustness of the technique make it a powerful single-molecule force spectroscopy assay that has become more and more popular in the academic community.

2 Description of a Magnetic Tweezers Apparatus

Magnetic tweezers for single-molecule studies are composed of a collimated light source located above a magnetic field source (e.g., permanent magnets) that is mounted on top of a flow cell in which super-paramagnetic beads (simply coined magnetic beads from now on) are tethered to the flow cell coverslip surface by a biomolecule (Fig. 1a). The magnetic beads are imaged using an inverted microscope onto a camera, which enables the tracking of their three-dimension position as a function of time. The latest complementary metal-oxide-semiconductor (CMOS) cameras enable both high-throughput (Fig. 1b) [24–27] and high-speed measurements [28–30]. The vertical and angular position of the magnets is adjusted using linear motors to vary the force (Fig. 1c) and the torque (Fig. 1d), respectively, applied to the biomolecule. The inverted microscope body may be either custom build or bought commercially. Given its simple design, the custom body presents only a mild difficulty to produce and is mechanically more stable.

2.1 Magnet Configuration

Different configurations have been used in magnetic tweezers experiments to modulate how force and torque are applied [15]. The most standard configuration uses a pair of cubic permanent magnets, being either vertically (Fig. 1a, c, and d) or horizontally aligned [31]. While the gap between the magnets gives access to the light source, it also modulates the applied force: a smaller gap results in a larger maximum force but reduces the surface area that experiences a homogenous force field [32, 33]. The

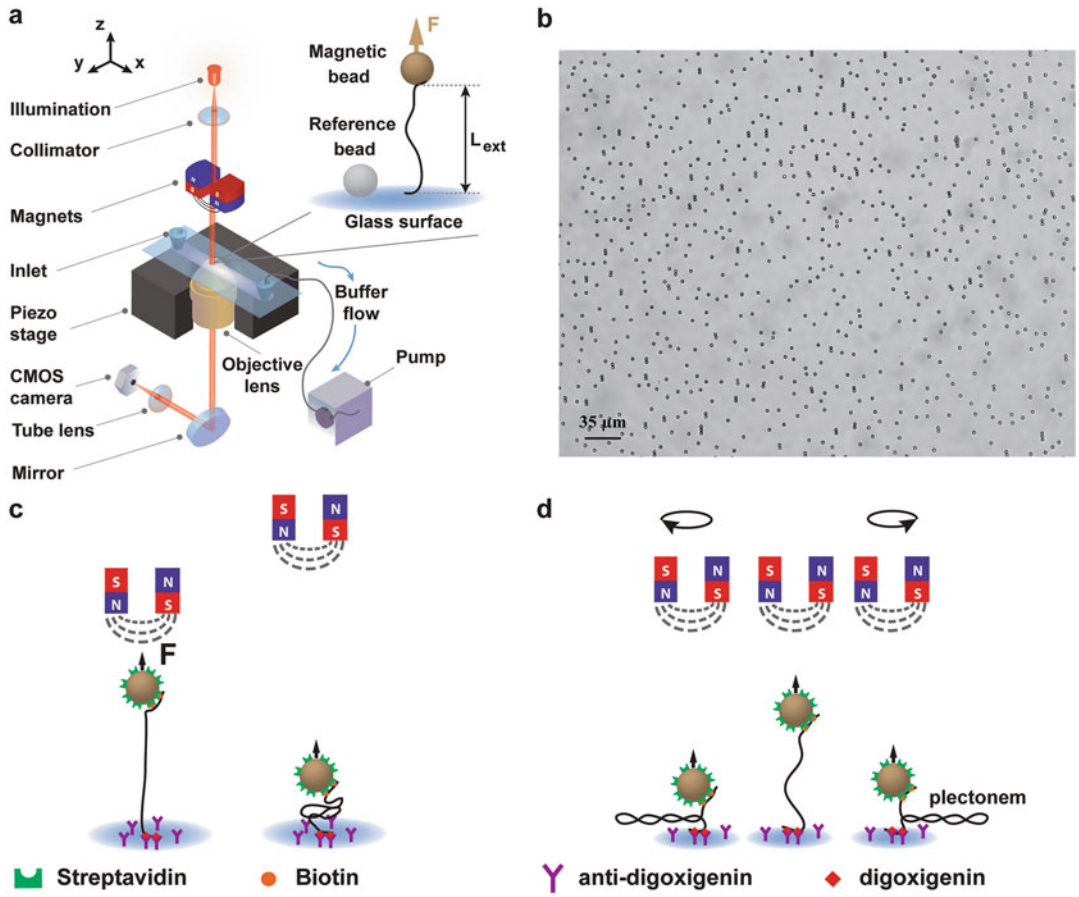

Fig. 1 Magnetic tweezers for single-molecule applications. (**a**) Schematic of a magnetic tweezers instrument (Adapted from Ref. [61]). (**b**) Field of view of a high-throughput magnetic tweezers assay, where ~500 magnetic beads of 2.8 μm diameter can be followed simultaneously (50× magnification, 120 nm pixel size) (Adapted from Ref. [49]). (**c**, **d**) Force and torque spectroscopy, respectively, of a single nucleic acid molecule using magnetic tweezers. The nucleic acid molecule is attached to the magnetic bead via a biotin-streptavidin bond, and to the surface via digoxigenin-antidigoxigenin attachment. Biotin and digoxigenin molecules are inserted nonspecifically during the synthesis of the nucleic acid handles that are subsequently ligated to the main nucleic acid strand (Adapted from Ref. [51])

two-permanent magnet cubes configuration strongly clamps the magnetic bead in rotation, which precludes specific applications, e.g., directly measuring the torsional stiffness of a soft biomolecule such as DNA. Alternative magnet geometries have therefore been developed using either a single cylindrical magnet [34] or additionally having a small side magnet attached to it to angularly trap the magnetic bead mildly [35, 36]. These methods have been reviewed in detail in Ref. [15].

2.2 Illumination

Different light sources have been used to illuminate the sample. A source is chosen to be spatially and temporally coherent, which generates many diffraction rings with a good contrast to enable an excellent tracking resolution. Light-emitting diodes (LEDs) are a simple solution that provide a good temporal coherence (~10 nm spectral dispersion, full width at half maximum), are easily collimated using a high numerical aperture aspherical lens, and provide enough light intensity to image the beads in standard image acquisition frequency (50–100 Hz) (Fig. 1a). To achieve high-speed image acquisition (≥ kHz), a high photon flux through the sample is required. Unfortunately, LEDs can hardly satisfy this requirement. With a noncoherent light source, a high flux may be achieved using a fiber-coupled arc lamp in combination with a spectral filter [30, 37]. Coherent sources such as laser diodes and superluminescent diodes also enable an efficient collection and collimation of the output light onto the sample [38]. This enables short camera shutter times and therefore high image acquisition rates. However, these coherent sources have the shortcoming of creating spurious speckle patterns in the field of view. Dark field illumination, i.e., by blocking the zero-order light pathway, has recently demonstrated the best to date resolution by reducing the background noise significantly [39].

2.3 Bead Position Tracking Algorithm

To follow biomolecular reactions with magnetic tweezers, one must precisely track the magnetic bead's position in three dimensions. To this end, different algorithms have been developed, all using the diffraction pattern originating from the out-of-focus micron-sized beads (Fig. 2a–c). A region of interest around the bead is defined a priori to indicate which area of the camera image contains single, insolated beads (Fig. 2a, b). A lookup table is acquired before the start of the experiment by capturing a diffraction pattern of the bead at different objective positions along the z-axis (Fig. 2a) [40, 41]. The objective is displaced using a high-resolution piezo stage in steps of ~50–100 nm (Fig. 1a). To determine the bead's position in the (x,y)-plane, a rough estimate is obtained from a center of mass, followed by a cross-correlation algorithm (Fig. 2d). More sophisticated versions of this tracking algorithm have been developed, such as the quadrant interpolation method [25, 42]. To determine the axial position (z-axis), the diffraction pattern of the magnetic bead at any given frame is compared to the lookup table using a squared error metric. Sub-plane resolution is then obtained by a polynomial fit of the resulting error curve (Fig. 2a). Because of the simplicity of these tracking algorithms, hundreds of beads may be followed in parallel and in real-time using modern GPUs to perform the calculation [25, 30].

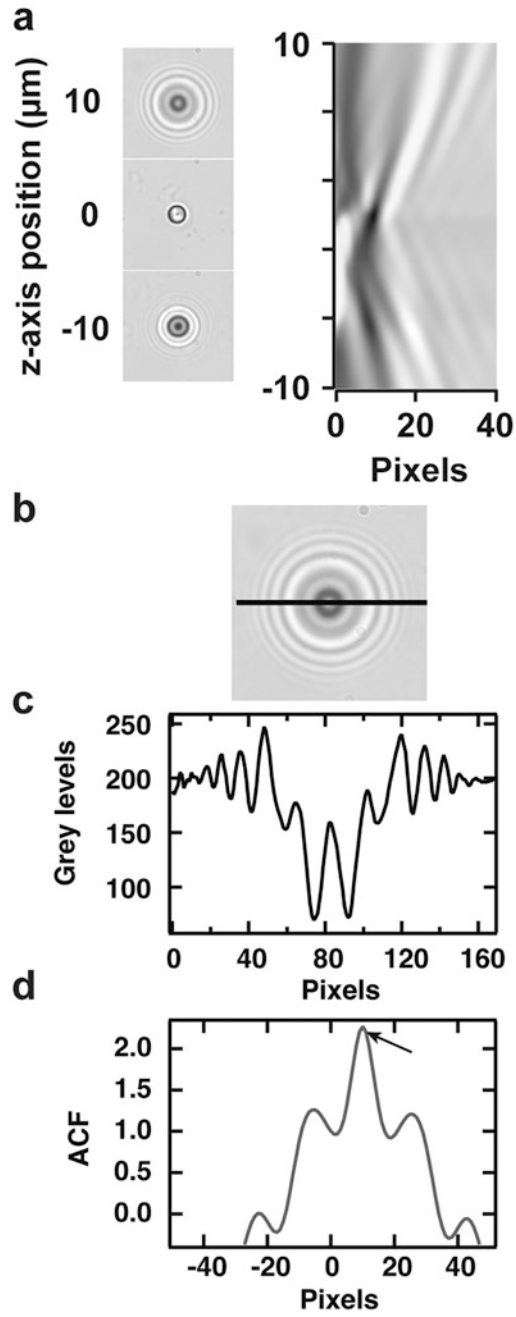

Fig. 2 Bead localization in a magnetic tweezers experiment. (**a**) Left, diffraction pattern of a 3 μm diameter reference bead attached to the surface of a coverslip at different distances from the bead to the microscope objective's focal plane along the *z*-axis. Right, a lookup table built up from radial intensity profiles across the center of the images of the diffraction pattern taken at different focal plane positions spaced by 50 nm intervals. (**b**, **c**) Diffraction pattern and intensity profile along the *x*-axis (black line). (**d**) Autocorrelation function (ACF) between two profiles as in (**b**) separated by 10 pixels (gray). The maximum of ACF is indicated by the arrow

2.4 Temperature Control

Enzymatic reactions are sensitive to temperature fluctuations and follow the Arrhenius law:

$$k(T) = Ae^{-E_a/k_B T}, \quad (1)$$

where k is the forward reaction rate constant, A is a pre-exponential factor, E_a is the activation energy, k_B the Boltzmann constant, and T the temperature [43]. It is therefore of great importance to precisely control the temperature in the flow chamber. Several articles have been reported on establishing a temperature control on the flow chambers [44–46]. Simulation and data have clearly demonstrated that the main heat sink is the oil immersion objective [45], which directly contacts with the glass coverslip area where the reaction occurs. In conclusion, controlling the temperature at the objective enables a precise control of the temperature of the reaction (±0.1 °C), which can be achieved using a simple device commercially available from Thorlabs [46].

2.5 Surface Functionalization and Nucleic Acid Construct Fabrication

Magnetic tweezers are a surface-based technique (Fig. 1a); therefore, the flow chamber's glass surface should be treated with care to prevent nonspecific attachment to the surface of either the magnetic beads or the biomolecules of interest. Different types of surface functionalization have been developed, such as polyethylene glycol (PEG) [47, 48], nitrocellulose [49], and lipid bilayer [50]. The last two are being described in detail in Chapter 21. The type of attachment is of great importance and therefore defines the methodology to generate the tether. The standard method of tethering the magnetic beads relies on fabricating nucleic acids containing both a biotin handle on one end, to attach the streptavidin coated bead, and a digoxigenin (dig) handle on the other end to attach the nucleic acid to anti-digoxigenin (anti-dig) antibodies adsorbed to the flow chamber's glass surface [51]. Such labels are introduced when generating the nucleic acid by adding dig- or biotin-labeled UTP to the nucleotide sets. While biotin-streptavidin forms a very stable bond, the dig-anti-dig bond is much weaker and not suitable for high-force or long experiments, even when using glutaraldehyde to cross-link proteins to the nitrocellulose surface [52]. For such experiments, covalent attachment is preferred to replace the dig-anti-dig bond using either a PEG functionalized surface with covalent chemistry to attach the biomolecule to the surface [47, 48] or a direct attachment [20], providing a tether with a much longer tether surface attachment lifetime .

DNA and RNA construct fabrication rely either on specific ligation of double-stranded ends (Fig. 3a, b), annealing single-stranded nucleic acids, or a combination of both. Very detailed protocols can be found in several method articles [51–56], and this topic will therefore not be further discussed here.

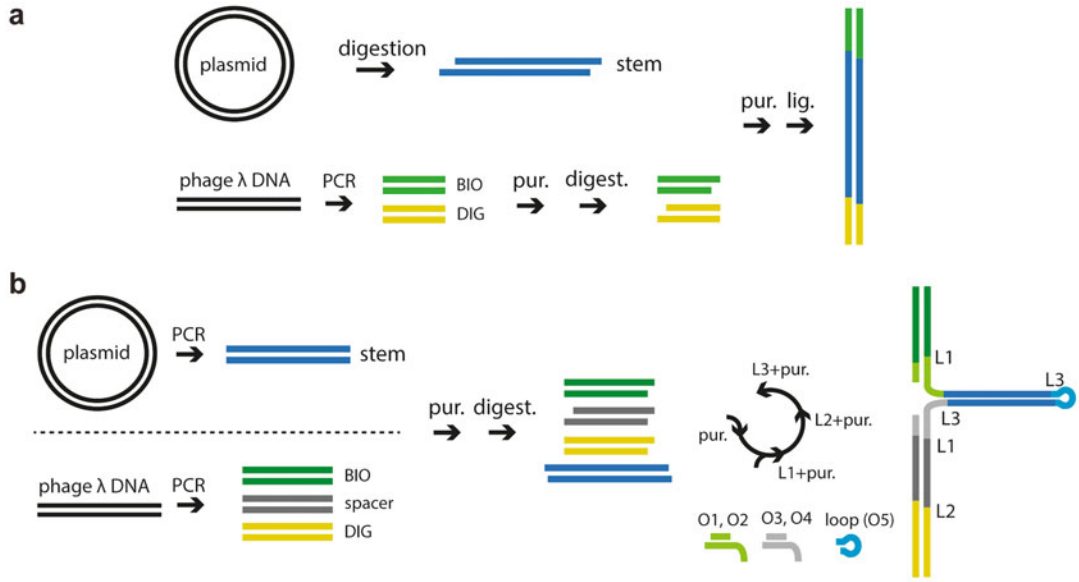

Fig. 3 DNA construct fabrication for single-molecule force spectroscopy experiments. (**a**) Steps in synthesizing double-stranded DNA constructs. A plasmid is digested to generate a stem. Handles labeled with either biotins (BIO) or digoxigenins (DIG) are generated by PCR using λ phage DNA as a template and by adding either bio-dUTP or dig-dUTP in the reaction solution. The handles are purified, digested, and ligated to the stem. (**b**) Similar approach as in (**a**) to fabricate a DNA hairpin. The different segments are produced by PCR digestion and ligated together to shape as a hairpin

3 Physical Principles

3.1 Force and Torque Origin

Magnetic tweezers can apply forces between a femto-Newton (fN) and a nano-Newton (nN) [4], which depends on the magnetic bead size (i.e., the total amount of magnetic content) and the magnet configuration. In the configuration described in Fig. 1a, reducing the gap between the two magnets increases the force. Because of the very large force range accessible, magnetic tweezers have been applied to investigate very different biomolecular systems. The force experienced by a magnetic particle in a magnetic field is described by:

$$\vec{F}_{\mathrm{mag}} = \frac{1}{2}\vec{\nabla}\left(\vec{m}_{\mathrm{sat}} \cdot \vec{B}\right), \tag{2}$$

where $\vec{F}_{\mathrm{mag}}$ is the magnetic force, $\vec{m}_{\mathrm{sat}}$ is the saturated magnetization of the particle, and $\vec{B}$ is the magnetic field [32]. Interestingly, the magnetic force is directly proportional to the gradient of the magnetic field, not its magnitude.

One of the key aspects of magnetic tweezers is their ability to apply torque to the tether [6, 57], and torque spectroscopy was performed on many different complexes, e.g., double-stranded

nucleic acids and nucleoprotein filaments [15]. The magnetic beads are made of super-paramagnetic nanoparticles embedded in a latex matrix, and therefore their magnetization should align with the magnetic field. However, an asymmetry in the nanoparticle spatial organization induces an anisotropy in $\vec{m}_{\text{sat}}$, with a minor component $\vec{m}_0$ not aligned with $\vec{B}$ [58]. This induces a torque $\vec{\Gamma}$ on the bead, which is derived from:

$$\vec{\Gamma} = \vec{m}_0 \times \vec{B}. \tag{3}$$

The torque response of the biomolecule is negligible in respect to $\vec{\Gamma}$. Hence, rotating the magnets induces a rotation of the magnetic bead, thereby transferring torque to the coilable tether. An example of coilable tether is a fully double-stranded nucleic acid molecule with multiple attachment points at both ends (Fig. 1a). To measure the torque response of the biomolecule, and therefore its torsional stiffness and related mechanical properties, different magnet configurations have been developed to reduce the magnitude of $\vec{\Gamma}$, such as the magnetic torque tweezers [35].

3.2 Force Calibration

The force F_{mag} may be calibrated from Eq. (1), by using m_{sat} (from the factory specifications of the magnetic beads) and spatially characterizing the magnetic field generated by the magnets with a Hall probe [32]. However, this method is not the preferred one, as it relies on parameters measured externally for a given batch of beads. Therefore, in situ force calibration methods that rely on parameters directly measured in the magnetic tweezers assay are preferred [59]. To this end, the theory relating the force as a function of the tethered magnetic bead lateral fluctuations is derived below. The force may therefore be extracted from measuring such fluctuations.

The position of a tethered magnetic bead experiencing a force F_{mag} is best described as an inverted pendulum (Fig. 4a, b) [6, 60] with two representative cases of pendulum lengths coined short (Fig. 4a) and long pendulum (Fig. 4b), respectively. In the former case, the fluctuation in position along the x-axis is pinned by the magnetic field $\vec{B}$ (Fig. 4a), and the length of the pendulum is therefore the length of the tether L_{ext}. In the latter case, the fluctuation in position of the bead along the y-axis is not constrained by the magnetic field (Fig. 4a), and the length of the pendulum is therefore $L_{\text{ext}} + R$, where R is the magnetic bead radius.

Considering the short pendulum case, the small displacement δx from the equilibrium position caused by the collisions with the water molecules (Fig. 4c), i.e., the Brownian motion, induces a restoring force that can be described as:

$$F_{\text{restoring}} = k_x \delta x, \tag{4}$$

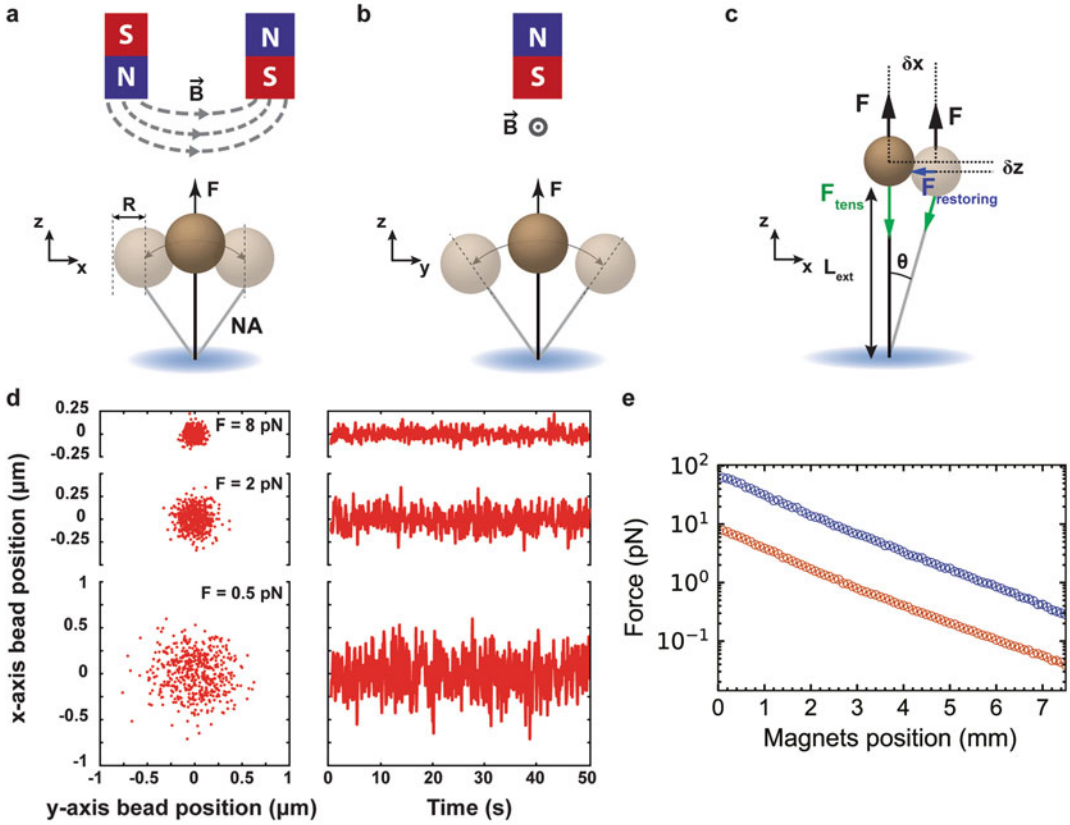

Fig. 4 Force calibration in a magnetic tweezers instrument. (**a**, **b**) Schematic of the tethered magnetic bead position fluctuations along either (**a**) the *x*-axis (short pendulum) or (**b**) the *y*-axis (long pendulum). (**c**) Schematic of the forces exerted on the magnetic bead in the short pendulum configuration. (**d**) Position of a magnetic bead along the *x*-axis against the *y*-position (left) and time (right). Data taken at three different forces. (**e**) Force calibration for M270 (blue, 2.8 μm diameter) and MyOne (red, 1 μm diameter) magnetic beads as a function of the distance of the magnets to the flow chamber (Adapted from Ref. [61])

where k_x is the trap stiffness along the *x*-axis. Therefore,

$$F_{\text{restoring}} = F_{\text{mag}} \cdot \sin(\theta) = F_{\text{mag}} \cdot \delta x / L_{\text{ext}}, \tag{5}$$

and

$$k_x = F_{\text{mag}} / L_{\text{ext}}, \tag{6}$$

where θ is the angle spanned by the tether when the bead is at its current and equilibrium positions, and L_{ext} is the length of tether. At small θ, the potential energy landscape U_{x} is quadratic [60], i.e.,

$$U_{\text{x}} = (1/2) \cdot k_{\text{x}} \delta x^2, \tag{7}$$

and we can therefore apply the equipartition theorem ($\langle U_{\text{x}} \rangle = (1/2) \cdot k_{\text{B}} T$) on Eq. (7), and we obtain:

$$\langle \delta x^2 \rangle = k_B T / k_x = k_B T \cdot L_{ext} / F_{mag}, \tag{8}$$

and, by extension, for the long pendulum case:

$$\langle \delta y^2 \rangle = k_B T / k_y = k_B T \cdot (L_{ext} + R) / F_{mag}. \tag{9}$$

Equation (8) and (9) directly link the applied force with the fluctuations in the lateral position of the bead and the tether length (Fig. 4d). Both are parameters that one can easily retrieve from experiments to enable a direct force calibration as a function of the distance of the magnets from the magnetic bead (Fig. 4e) [61, 62].

To provide an accurate force calibration, the lateral fluctuation of the bead must be measured accurately to not overestimate the force (Eqs. 8 and 9). To this end, one should make sure the image acquisition does not overly integrate (meaning average) the magnetic bead position fluctuation [61]. From the equation of motion of the magnetic bead experiencing F_{mag}, we are able to extract the characteristic time scale of the bead:

$$\begin{aligned} t_{c,x} &= \gamma / k_x = 6\pi\eta R L_{ext} / F_{mag} \text{ and } t_{c,y} = \gamma / k_y \\ &= 6\pi\eta R (L_{ext} + R) / F_{mag}, \end{aligned} \tag{10}$$

where γ is the drag coefficient, η the viscosity of the solution (typically water, i.e., ~10^{-3} Pa.s), and R the radius of the magnetic bead and defines the time during which the bead has explored the trap. For $L_{ext} \leq R$, the drag coefficient must be corrected to include the effect of the surface, as described by the Faxén law [63]:

$$\gamma_{Faxen} = 6\pi\eta R \Big/ \left[\begin{array}{l} 1 - 9/8(R/(R+L_{ext})) + 1/2(R/(R+L_{ext}))^3 - 57/100(R/(R+L_{ext}))^4 \\ +1/5(R/(R+L_{ext}))^5 + 7/200(R/(R+L_{ext}))^{11} - 1/25(R/(R+L_{ext}))^{12} \end{array} \right], \tag{11}$$

$\langle \delta x^2 \rangle$ averages away toward a measured value $\langle \delta x^2 \rangle_{meas}$ as a function of the camera shutter time τ_{sh} and $t_{c,\,x}$ as

$$\langle \delta x^2 \rangle_{meas} = (2 k_B T / \pi k_x) \arctan\left(4\pi t_{c,x} / \tau_{sh}\right). \tag{12}$$

To minimize the error in the force due to camera image blurring, we must minimize the difference between $\langle \delta x^2 \rangle$ and $\langle \delta x^2 \rangle_{meas}$. For example, to measure F_{mag} with a 10% error due to camera image blurring, τ_{sh} must be at least four times smaller than $t_{c,\,x}$ [61]. How feasible is this in practice? Most large chip CMOS cameras acquire images with a frequency f_{ac}~10 − 100 Hz, while the characteristic time for a L_{ext} = 1 μm, R = 1.4 μm and F_{mag} = 10 pN (typical experimental conditions) is $t_{c,\,x}$~0.03 s, i.e., similar to τ_{sh} for zero-dead time image acquisition ($f_{ac} \sim 1/\tau_{sh}$). In such case, one may use longer DNA tethers to increase $t_{c,\,x}$ in respect of τ_{sh} and extract a calibration table for F_{mag} as a function of the magnets distance to the magnetic bead [59]. However, this only works for magnetic beads with a small dispersion in magnetic content, hence in force, such as the Dynabeads M-270 (R = 1.4 μm) and MyOne (R = 0.5 μm) magnetic beads from

Invitrogen. For shorter tethers or higher forces, one may use a very fast camera, i.e., f_{ac} in the kilohertz range, or use a nonzero dead time acquisition, i.e., $\tau_{sh} \ll 1/f_{ac}$ [59, 61]. The former is not available for all camera models and only when using a small field of view [28–30].The latter is easily programmable in most cameras without compromising the field of view [61]. Another possibility is to correct $\langle \delta x^2 \rangle_{meas}$ for the camera image blurring, either in the frequency or time domain [59, 64]. This works well for $\tau_{sh}/2 < t_{c,x} < \tau_{sh}/4$ [60], and packages in MATLAB and Python are available to perform such calibrations [59, 65]. These strategies however fail to perform accurate force calibration for very short tethers, as the rotation of the bead induced by the magnetic field pinning by the magnetic bead must be accounted for [66, 67]. Similar strategies to calibrate the force may also be applied to acoustic force spectroscopy (AFS) [68], as the tethered bead is described by a similar model (i.e., the inverted pendulum).

3.3 Estimating the Spatiotemporal Resolution of Magnetic Tweezers

The main parameters measured in magnetic tweezers experiments are the change in the tether's extension L_{ext} due to either a mechanical response of the tether or an enzymatic activity modifying the tether length. It is therefore essential to determine the noise amplitude along the z-axis. The spatiotemporal resolution in a magnetic tweezers assay depends on the tracking and thermal noise as follows:

$$\langle \delta z_{tot} \rangle = \sqrt{\delta z_{tr}{}^2 + \delta z_{th}{}^2}. \tag{13}$$

3.3.1 Tracking Resolution and Stability

The tracking resolution is defined by the hardware (microscope objective magnification, numerical aperture, pixel size and light intensity) and the algorithm used. To experimentally evaluate δz_{tr}, the Allan deviation (AD) is particularly useful [28, 64, 69] (Fig. 5a). The AD of a particle position along the, e.g., z-axis, is defined as follows:

$$\sigma_{AD}(\tau) = \sqrt{\frac{1}{2}\left\langle \left(\overline{z}_{\tau,j+1} - \overline{z}_{\tau,j}\right)^2 \right\rangle} \text{ with } \overline{z}_{\tau,j} = \frac{1}{\tau}\int_{\tau(j-0.5)}^{\tau(j+0.5)} z(t)dt, \tag{14}$$

where τ defines both the time between consecutive samples and the time over which the sample is averaged. Simply put, the AD is one-half the average difference in position between consecutive intervals of duration τ, averaged over all intervals of duration τ. For a bead stuck to the surface, we observe two regimes (Fig. 5a): AD initially decreases as $1/\sqrt{\tau}$, indicating how the frame-to-frame uncorrelated noise averages out, and the AD subsequently reaches a lower bound and rises again due to long timescale drift dominating the noise (e.g., mechanical drift, tracking algorithm bias). To improve the stability during the measurement, the mechanical drift is corrected by subtracting the position of a reference bead

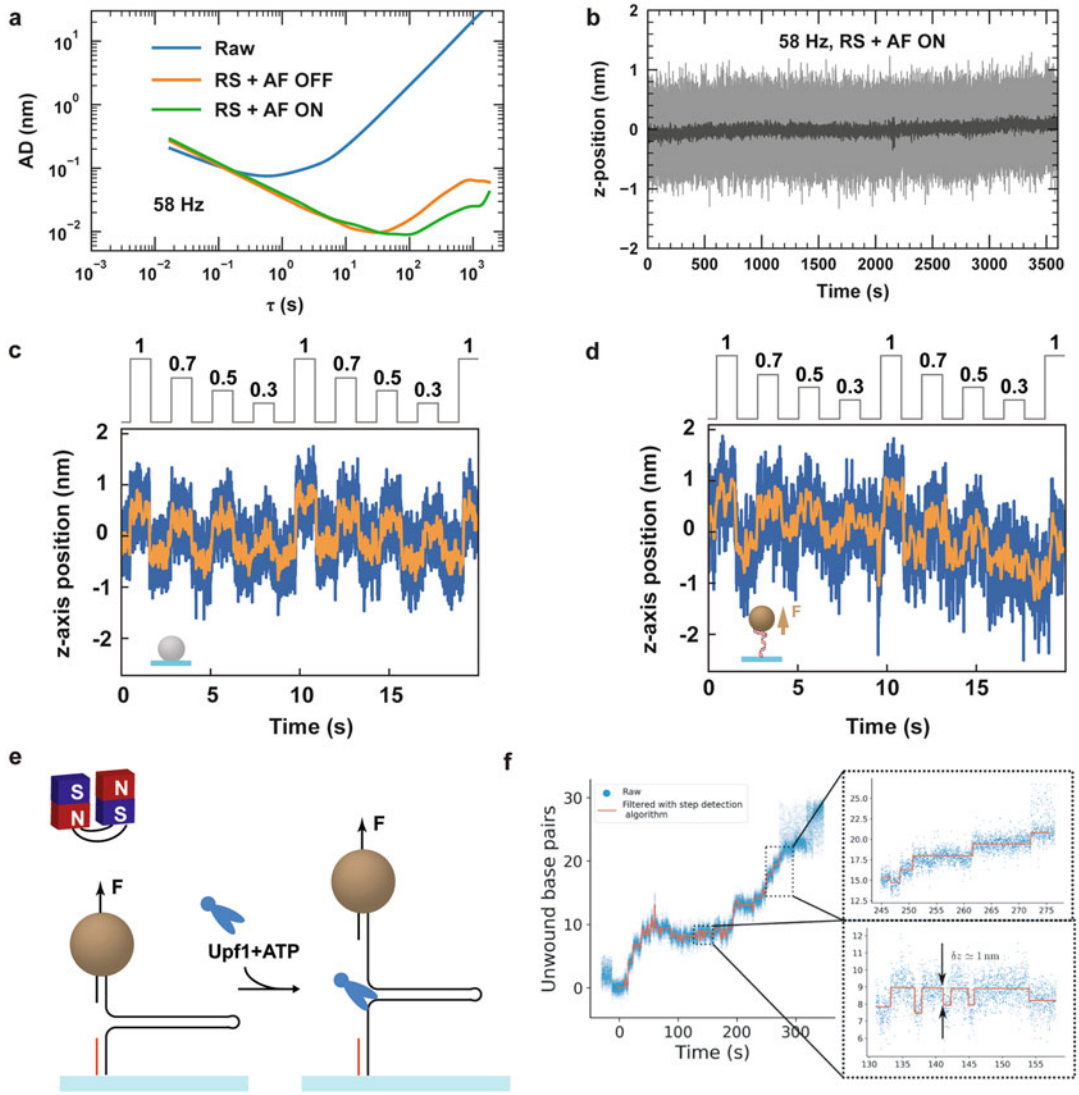

Fig. 5 Spatiotemporal resolution of a magnetic tweezers instrument. (**a**) Allan deviation (AD) of the *z*-axis position of a 3 μm diameter surface-attached polystyrene reference bead (blue), subtracted to another reference bead (RS, orange), and using autofocus (AF, green). The data were acquired using a 100× objective magnification and at 58 Hz acquisition frequency. (**b**) Raw (gray) and 1 Hz low-pass filtered (dark gray) trace acquired while using the autofocus and drift corrected by subtracting the *z*-position of another reference bead (green in (**a**)) (Adapted from Ref. [49]). (**c**, **d**) Height of a (**c**) reference bead and (**d**) DNA-tethered bead while using the piezo stage to move the sample by the increments indicated on top of the panel (in nm) (Adapted from Ref. [69]). (**e**, **f**) Magnetic tweezers assay to monitor single-nucleotide steps of Upf1 helicase when unwinding a DNA hairpin (Adapted from Ref. [39])

fixed to the flow chamber surface from the position of the magnetic bead (Figs. 1a and 5a) [28]. The resolution of the bead position tracking may be further improved by setting an autofocus locked onto the position of a reference bead and adjusting the objective's

focal plane's position using a high-resolution piezo stage and increase the τ at which AD rises again by decreasing the negative impact of the tracking algorithm bias [49] (Fig. 5a, b). For a magnetic tweezers instrument with 100× magnification, 1.25 numerical aperture microscope objective, and 60 nm pixel size in the image plane, tracking resolutions for a single image of δz_{tr}~1 nm and δz_{tr}~0.3 nm are achievable for 1 μm and 3 μm diameter beads, respectively (using the quadrant interpolation algorithm) [69].

The tracking resolution may be improved by acquiring data at high f_{ac} and subsequently averaging out the tracking noise by integrating the bead position over N frames. This results in a reduction of the tracking noise by a factor of $\sqrt{N}$, enabling the observation of steps as small as 0.3 nm for a reference bead with the standard magnetic tweezers configuration (Fig. 5c) [28–30, 69] and for a tethered magnetic bead (Fig. 5d) [69]. Recent developments in magnetic tweezers instrumentation, specifically in the illumination and imaging path, have enabled the first observation of single-nucleotide translocation steps by a helicase unwinding a DNA hairpin (Fig. 5e, f) [39].

3.3.2 Thermal Noise

The thermal noise depends on the tether stiffness, k_z, as follows:

$$\left\langle \delta z_{th}^2 \right\rangle = k_B T / k_z, \tag{15}$$

where

$$k_z = \frac{\partial F_{mag}(L_{ext})}{\partial L_{ext}} = \frac{k_B T}{2 L_P L_C} \left(2 + \left(1 - \frac{L_{ext}}{L_C} \right) \right) \tag{16}$$

with L_P and L_C being the persistence and the contour length of the tether, respectively, assuming the response of the tether to F_{mag} is well-described by the inextensible Worm-like chain model [70]. Similar to $\langle \delta x^2 \rangle_{meas}$, the thermal noise is integrated by the camera during the image acquisition. Hence,

$$\left\langle \delta z_{th}^2 \right\rangle_{meas} = (2 k_B T / \pi k_z) \ \arctan\left(4 \pi t_{c,z} / \tau_{sh} \right) \tag{17}$$

with $t_{c,\,z} = \gamma / k_z$. For $L_{ext} \leq R$, γ must be corrected to account for the coverslip surface effect using Brenner's approximation [63]:

$$\gamma_{Brenner} = 6 \pi \eta R / \Big[1 - 9/8 (R/(R + L_{ext})) + 3/8 (R/(R + L_{ext}))^3 - 1/4 (R/(R + L_{ext}))^4 \Big], \tag{18}$$

Ideally, the resolution of the magnetic tweezers assay is limited by the thermal noise, which can be estimated using Eqs. 16 and 17. An accurate simulation of the overall measurement noise for a tethered magnetic bead in a magnetic tweezers assay has been described by Burnham and colleagues [71], which is useful to

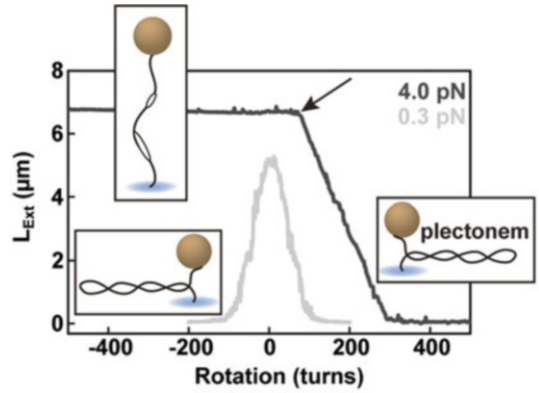

Fig. 6 DNA supercoiling experiments using magnetic tweezers. Dynamic rotation-extension experiment on a 21 kbp long DNA tether at either 0.3 pN (gray) or 4 pN (black). At low force, both negative and positive supercoils induce plectonemes. At high force, positive supercoils induce plectonemes, while negative supercoils unwind the DNA tether. The arrow indicates the buckling transition at high force

estimate the spatiotemporal resolution for a given magnetic tweezers experiment.

3.4 Using Torque Spectroscopy in Magnetic Tweezers

One of the key aspects of magnetic tweezers is their ability to control the torque applied to a coilable biomolecule (Fig. 1d, Fig. 6) [6, 57]. This has been (and still is) used to investigate the mechanical response to torque of double-stranded nucleic acids [15, 72]. To enable torque spectroscopy, the nucleic acid must be topologically constrained, i.e., without free rotation point, such as a fully double-stranded DNA with multiple attachment points at both ends (Fig. 1d). The twist (Tw) and the writhe (Wr) define the supercoiled state of the molecule. The former is the number of times the molecule turns around itself, such as for the DNA double helix, and the latter is defined by the number of times the molecule winds over itself. The helical pitch for a relaxed DNA molecule is 10.5 bp/turn and, therefore, the total twist in a relaxed DNA molecule (Tw_0) is the number of base pairs divided by the helical pitch. The linking number (Lk), which is the sum of twist and writhe, is a topological invariant for a torsionally constrained molecule, meaning

$$Lk = Tw + Wr = \text{constant}. \tag{19}$$

For a torsionally relaxed DNA molecule, $Wr = 0$, so $Lk_0 = Tw_0$. A molecule is said to be supercoiled when $Lk \neq Lk_0$.

In addition, the supercoil density σ is a useful description of the torsional state of a molecule:

$$\sigma = (\mathrm{Lk} - \mathrm{Lk}_0)/\mathrm{Lk}_0. \quad (20)$$

L_{ext} as a function of σ is often used to represent magnetic tweezers experiments investigating the response of double-stranded nucleic acids to torsional stress. This provides an easy way to compare the torsional properties of DNA tethers of different lengths.

Upon addition of positive turns to a torsionally relaxed molecule, L_{ext} remains constant at first, as the addition of twist is absorbed through deformation of the molecule (Fig. 6). In this regime, $\mathrm{Tw} > \mathrm{Tw}_0$, $\mathrm{Wr} = 0$, and the torque Γ increase linearly with the number of turns N:

$$\Gamma = C2\pi N/L_C, \quad (21)$$

where C is the torsional modulus of the molecule, e.g., C~90 k_BT for DNA [35, 73–75]. This may be used to monitor the torque-dependence of a specific DNA-protein interaction, e.g., RNA polymerase-promoter open complex formation by the bacterial RNA polymerase [76]. At the critical torque Γ_C, the molecule's extension suddenly decreases to form the first loop upon further addition of coiling to the DNA molecule (Fig. 6). This event is also called the buckling transition and is followed by a linear decrease in L_{ext} with added turns [6, 77]. Γ_C is given through having the energy to form a loop of radius R_L being equal to the work done by the addition of one extra turn $2\pi\Gamma_C$:

$$E_R = 2\pi R_L F_{mag} + \pi L_P k_B T/R_L, \quad (22)$$

Minimizing E_R as a function of R_L gives Γ_C and the change in extension per superhelical turn Δz such as [73, 78]:

$$\Gamma_C = \sqrt{2L_P k_B T F_{mag}} \text{ and} \Delta z = 2\pi R_L = \pi\sqrt{2L_P k_B T/F_{mag}}, \quad (23)$$

This model only describes Δz qualitatively, and more sophisticated models have been derived to describe Δz more accurately [15, 31]. At high force and in the negative supercoil regime, it is more favorable for the DNA molecule to unwind than forming plectoneme, while the rotation-extension of a DNA molecule is symmetrical at low force, i.e., the tether forms plectonemes for both negative and positive supercoil addition (Fig. 6).

4 Combining Magnetic Tweezers with Other Techniques

Magnetic tweezers have been combined with fluorescence microscopy to enable simultaneous force/torque and fluorescence spectroscopy investigations. The preferred fluorescence approach is objective-based total internal reflection fluorescence microscopy (TIRFM), as it is a surface-based approach with a shallow excitation depth (~hundreds of nanometers), leaving the magnetic bead out

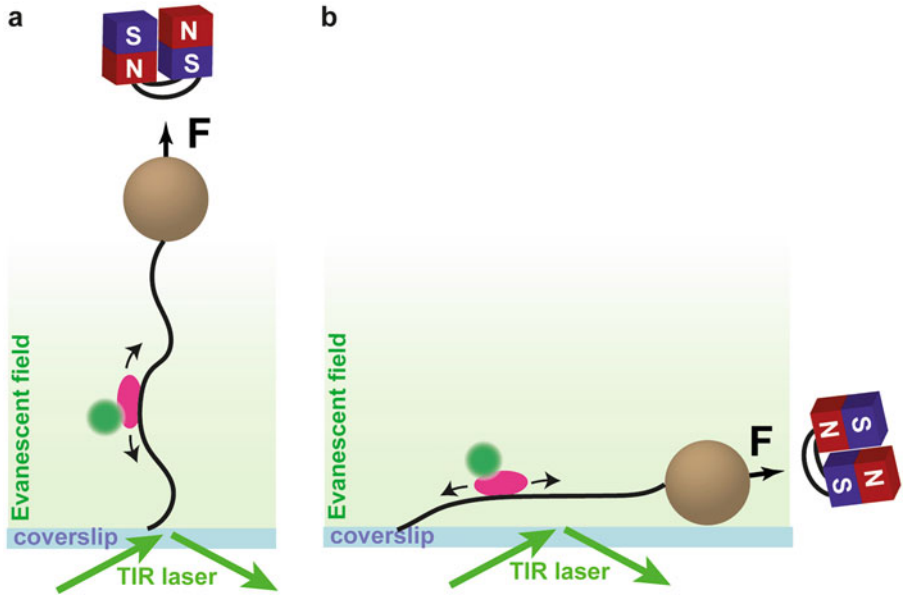

Fig. 7 Magnetic tweezers combined with total internal reflection fluorescence (TIRF) microscopy. (**a**) Vertically oriented attractive force and (**b**) horizontally oriented attractive force. The pink oval indicates a protein of interest labeled with a fluorescent dye (green sphere). In (**a**), the exponential decay of the evanescent field is used to localize the protein along the DNA, while in (**b**) the position is determined from direct localization in the plane of observation

of the excitation volume. Two main configurations have been reported for such assay, using either a standard vertical magnet configuration (Fig. 7a) or a horizontal magnet configuration (Fig. 7b). In the former configuration, the magnets pull vertically on the magnetic bead, and vertical motion of a dye-labeled enzyme may be reported using the fluorescence channel and the exponential decay of the evanescent field of the TIRF excitation [79–82]. In the latter configuration, a magnetic force is applied sideways, which stretches the DNA molecule laterally, enabling transverse observation of displacements biomolecular objects (e.g., protein, plectoneme) [83–85]. These two configurations have different advantages. The first enables rapid modulation of the applied torque, as is done in the rotor bead assay developed by Bryant and colleagues [12]. A sideway configuration gives access to a higher localization precision of fluorescently labeled biomolecules moving along, e.g., a DNA tether [83–85]. Chapter 22 will discuss different configurations of magnetic tweezers combined with fluorescence microscopy. Darkfield microscopy has been combined with magnetic tweezers in the rotor bead assay to use backscattered light from a gold nanoparticle as a tracker, which provides an excellent signal-to-noise ratio while minimizing the size of the object to track, and therefore gives access to a higher measurement bandwidth [86]. The combination of magnetic tweezers with optical tweezers has also been reported by Cees Dekker and colleagues [87].

5 Applications of Magnetic Tweezers in Single-Molecule Biophysics

Magnetic tweezers present many advantages to study biomolecules in vitro one at a time. They are a force clamp technique that enables force spectroscopy measurements from ~10 fN to ~1 nN [4], depending on the total amount of magnetic material in the bead. Because the distance between the magnetic bead and the magnets has to vary significantly (around 0.05 mm) to vary the force significantly, magnetic tweezers can apply a constant force over very long measurement. This holds true even at low force (< 1 pN), unlike for an AFM or optical tweezers. Furthermore, the combination of a homogenous magnetic field over a very large field of view (~mm^2) and commercially available magnetic beads with homogenous magnetic content enables high-throughput force spectroscopy measurements at constant force with a small bead-to-bead variation in force (~10% standard deviation). For these reasons, magnetic tweezers have been applied to study protein folding and unfolding dynamics at a low constant force [19], such as the titin immunoglobulin domain [23], talin and protein L [21], von Willebrand factor folding [20], protein-ligand interactions to interrogate either SARS-CoV-2 spike or ACE2 interactions (Fig. 8a, b) [88], and the rapamycin-mediated association between FKBP12 and FRB [22, 89].

Furthermore, the recent advances in tracking algorithms, illumination, and imaging strategies have brought magnetic tweezers on par with optical tweezers in terms of their spatiotemporal resolution. Additionally, the ability to perform high-throughput tracking in magnetic tweezers enables the in-depth characterization of mechanochemical pathways of translocating molecular motor. Examples include viral RNA polymerases (Fig. 8c, d) [26, 49, 90–92], the bacterial RNA polymerase [93], the DNA polymerase [7, 8], helicases (Fig. 5c) [39, 44, 94–104], and the SMC complex [105, 106]. Magnetic tweezers have also enabled the characterization of nucleoprotein filament formation or mechanical properties [107–110], protein-mediated DNA condensation [111, 112], and chromatin filament and nucleosome stability [113–117].

Magnetic tweezers are naturally well suited to perform torque spectroscopy experiments. This has been extensively used to investigate biological systems that induce a change in the linking number of a tethered coilable double-stranded nucleic acid. Topoisomerases remove the excess of negative or positive supercoils in the DNA molecule that naturally occur in the cell during DNA transcription and replication [118]. Therefore, their activity is essential to maintain cellular homeostasis. Using magnetic tweezers to induce a large excess of supercoils to a DNA molecule has been used to investigate the mechanochemical cycle of topoisomerases [24, 119–124]. Cellular RNA polymerases have been extensively

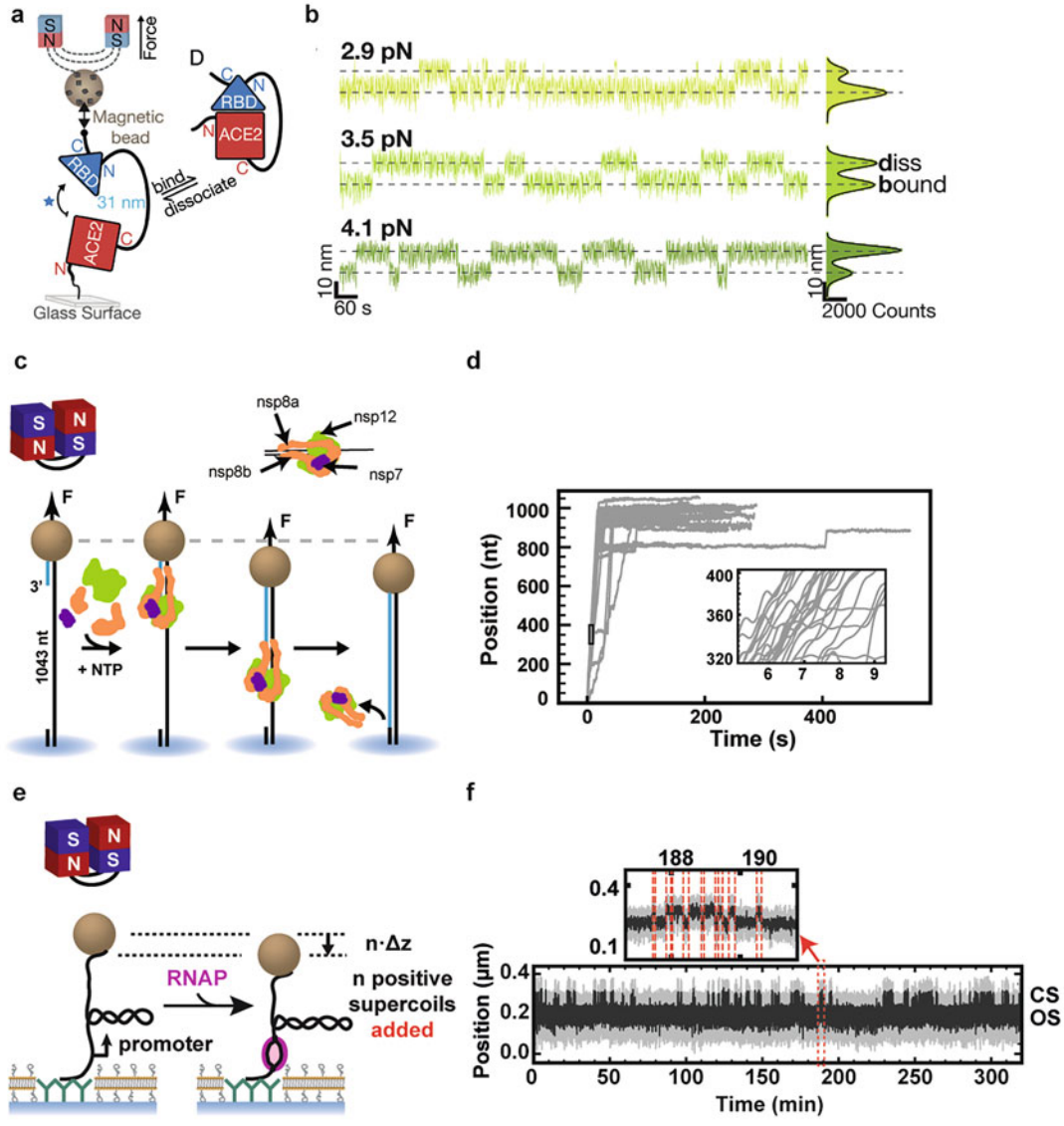

Fig. 8 Examples of magnetic tweezers applications in single-molecule biophysics. (**a**, **b**) Schematic and experimental traces showing the binding and dissociation kinetics of the SARS-CoV-2 spike protein RBD from the ACE2 receptor as a function of force. (**b**) The time-dependent traces reveal populations in the bound and dissociated states as a function of the applied force (Adapted from Ref. [88]). (**c**, **d**) Schematic and experimental traces of elongating SARS-CoV-2 core replication-transcription complexes. (**d**) The time-dependent traces demonstrate rich dynamics with bursts of nucleotide addition interrupted by pauses of various durations (Adapted from Ref. [49]). (**e**, **f**) RNA polymerase (RNAP)-promoter open complex formation on a positively supercoiled DNA. Upon promoter opening, upon n positive supercoils addition, moving the bead downward by $n\Delta z$. The surface is passivated using a lipid-bilayer strategy. The trace in (**f**) shows the promoter alternating between a closed state (CS, promoter closed) and an open state (OS, RNAP-promoter open) (Adapted from Ref. [50])

investigated using magnetic tweezers. Indeed, they must open double-stranded DNA at the promoter site to form the RNA polymerase-promoter open complex and initiate transcription, which consequently removes ~1 turn of twist in the DNA molecule (the transcription bubble is 13–14 nt, and DNA makes one full turn every ~10.5 bp). Using the conservation of the linking number condition described above (Fig. 8e), many details in the mechanism of transcription initiation by cellular RNA polymerase have been revealed (Fig. 8f), such as the impact of torque on promoter opening, the dynamics of transcription initiation and promoter escape as a function of the promoter sequence and salt concentration, the transcription start site selection, and R-loop formation during transcription [14, 50, 76, 125–129]. A similar approach was used to investigate Cas9 R-loop formation [130, 131]. The torque spectroscopy capabilities of magnetic tweezers have also been used to investigate the torsional properties and stability of chromatin filaments [116, 132, 133] and nucleosome assembly [134–136], as well as other nucleoprotein filaments, such as those formed by Rad51, RecA, and H-NS [35, 137–141].

6 Perspectives

The unique advantages of magnetic tweezers, i.e., simplicity (and therefore low cost), stability, high parallelization and resolution, large force range, and torque spectroscopy, make it a very powerful technique. It has been established in many labs worldwide, with an ever-increasing demand. Only one company currently sells magnetic tweezers instruments (Mad City labs), and more could be done to have the technique more available at low cost. Currently, no open-source instrument design has been released or published, and CAD drawings would help democratizing magnetic tweezers. A software interface already exists [25], though in proprietary format (LabView, National Instruments), and efforts must be made to release an open-source interface in a nonproprietary language, such as Python. The development of routines for data analysis in nonproprietary languages to help the analysis of complex dynamics of molecular motors will further support the democratization of magnetic tweezers with appropriate statistical tools to analyze single-molecule data. Altogether, these developments will bring magnetic tweezers and their application to a broader community. Lastly, there is no combined high-throughput single-molecule force/torque and fluorescence spectroscopy assay available to date. The statistical power of such hydrid assay would potentiate the investigation of ever more complex biomolecular systems.

References

1. Crick FHC, Hughes AFW (1950) The physical properties of cytoplasm: a study by means of the magnetic particle method part I. Exp Cell Res 1(1):37–80. https://doi.org/10.1016/0014-4827(50)90048-6
2. Kah D, Durrbeck C, Schneider W, Fabry B, Gerum RC (2020) High-force magnetic tweezers with hysteresis-free force feedback. Biophys J 119(1):15–23. https://doi.org/10.1016/j.bpj.2020.05.018
3. Kollmannsberger P, Fabry B (2007) BaHigh-force magnetic tweezers with force feedback for biological applications. Rev Sci Instrum 78(11):114301. https://doi.org/10.1063/1.2804771
4. Dulin D, Lipfert J, Moolman MC, Dekker NH (2013) Studying genomic processes at the single-molecule level: introducing the tools and applications. Nat Rev Genet 14(1):9–22. https://doi.org/10.1038/nrg3316
5. Smith SB, Finzi L, Bustamante C (1992) Direct mechanical measurements of the elasticity of single DNA molecules by using magnetic beads. Science (New York, NY) 258(5085):1122–1126
6. Strick TR, Allemand JF, Bensimon D, Bensimon A, Croquette V (1996) The elasticity of a single supercoiled DNA molecule. Science (New York, NY) 271(5257):1835–1837
7. Manosas M, Spiering MM, Ding F, Croquette V, Benkovic SJ (2012) Collaborative coupling between polymerase and helicase for leading-strand synthesis. Nucleic Acids Res 40(13):6187–6198. https://doi.org/10.1093/nar/gks254
8. Manosas M, Spiering MM, Ding F, Bensimon D, Allemand JF, Benkovic SJ, Croquette V (2012) Mechanism of strand displacement synthesis by DNA replicative polymerases. Nucleic Acids Res 40(13):6174–6186. https://doi.org/10.1093/nar/gks253
9. Maier B, Bensimon D, Croquette V (2000) Replication by a single DNA polymerase of a stretched single-stranded DNA. Proc Natl Acad Sci U S A 97(22):12002–12007. https://doi.org/10.1073/pnas.97.22.12002
10. Charvin G, Strick TR, Bensimon D, Croquette V (2005) Tracking topoisomerase activity at the single-molecule level. Annu Rev Biophys Biomol Struct 34:201–219. https://doi.org/10.1146/annurev.biophys.34.040204.144433
11. Spakman D, Bakx JAM, Biebricher Andreas S, Peterman EJG, Wuite GJL, King Graeme A (2021) Unravelling the mechanisms of Type 1A topoisomerases using single-molecule approaches. Nucleic Acids Res 49(10):5470–5492. https://doi.org/10.1093/nar/gkab239
12. Basu A, Hobson M, Lebel P, Fernandes LE, Tretter EM, Berger JM, Bryant Z (2018) Dynamic coupling between conformations and nucleotide states in DNA gyrase. Nat Chem Biol 14(6):565–574. https://doi.org/10.1038/s41589-018-0037-0
13. McKie SJ, Neuman KC, Maxwell A (2021) DNA topoisomerases: advances in understanding of cellular roles and multi-protein complexes via structure-function analysis. BioEssays 43(4):e2000286. https://doi.org/10.1002/bies.202000286
14. Ostrofet E, Papini FS, Malinen AM, Dulin D (2019) A single-molecule view on cellular and viral RNA synthesis. In: Joo C, Rueda D (eds) Biophysics of RNA-protein interactions, Biological and Medical Physics, Biomedical Engineering. Springer, New York, pp 109–141. https://doi.org/10.1007/978-1-4939-9726-8
15. Kriegel F, Ermann N, Lipfert J (2017) Probing the mechanical properties, conformational changes, and interactions of nucleic acids with magnetic tweezers. J Struct Biol 197(1):26–36. https://doi.org/10.1016/j.jsb.2016.06.022
16. De Vlaminck I, Dekker C (2012) Recent advances in magnetic tweezers. Annu Rev Biophys 41:453–472. https://doi.org/10.1146/annurev-biophys-122311-100544
17. Morati F, Modesti M (2021) Insights into the control of RAD51 nucleoprotein filament dynamics from single-molecule studies. Curr Opin Genet Dev 71:182–187. https://doi.org/10.1016/j.gde.2021.09.001
18. Winardhi RS, Yan J (2017) Applications of magnetic tweezers to studies of NAPs. Methods Mol Biol 1624:173–191. https://doi.org/10.1007/978-1-4939-7098-8_14
19. Zhao X, Zeng X, Lu C, Yan J (2017) Studying the mechanical responses of proteins using magnetic tweezers. Nanotechnology 28(41):414002. https://doi.org/10.1088/1361-6528/aa837e
20. Lof A, Walker PU, Sedlak SM, Gruber S, Obser T, Brehm MA, Benoit M, Lipfert J (2019) Multiplexed protein force spectroscopy reveals equilibrium protein folding

dynamics and the low-force response of von Willebrand factor. Proc Natl Acad Sci U S A 116(38):18798–18807. https://doi.org/10.1073/pnas.1901794116

21. Tapia-Rojo R, Eckels EC, Fernandez JM (2019) Ephemeral states in protein folding under force captured with a magnetic tweezers design. Proc Natl Acad Sci U S A 116(16):7873–7878. https://doi.org/10.1073/pnas.1821284116
22. Kostrz D, Wayment-Steele HK, Wang JL, Follenfant M, Pande VS, Strick TR, Gosse C (2019) A modular DNA scaffold to study protein-protein interactions at single-molecule resolution. Nat Nanotechnol 14(10):988–993. https://doi.org/10.1038/s41565-019-0542-7
23. Chen H, Yuan G, Winardhi RS, Yao M, Popa I, Fernandez JM, Yan J (2015) Dynamics of equilibrium folding and unfolding transitions of titin immunoglobulin domain under constant forces. J Am Chem Soc 137(10):3540–3546. https://doi.org/10.1021/ja5119368
24. Agarwal R, Duderstadt KE (2020) Multiplex flow magnetic tweezers reveal rare enzymatic events with single molecule precision. Nat Commun 11(1):4714. https://doi.org/10.1038/s41467-020-18456-y
25. Cnossen JP, Dulin D, Dekker NH (2014) An optimized software framework for real-time, high-throughput tracking of spherical beads. Rev Sci Instrum 85(10):103712. https://doi.org/10.1063/1.4898178
26. Dulin D, Vilfan ID, Berghuis BA, Hage S, Bamford DH, Poranen MM, Depken M, Dekker NH (2015) Elongation-competent pauses govern the fidelity of a viral RNA-dependent RNA polymerase. Cell Rep 10(6):983–992. https://doi.org/10.1016/j.celrep.2015.01.031
27. Berghuis BA, Dulin D, Xu ZQ, van Laar T, Cross B, Janissen R, Jergic S, Dixon NE, Depken M, Dekker NH (2015) Strand separation establishes a sustained lock at the Tus-Ter replication fork barrier. Nat Chem Biol 11(8):579–585. https://doi.org/10.1038/nchembio.1857
28. Dulin D, Cui TJ, Cnossen J, Docter MW, Lipfert J, Dekker NH (2015) High spatiotemporal-resolution magnetic tweezers: calibration and applications for DNA dynamics. Biophys J 109(10):2113–2125. https://doi.org/10.1016/j.bpj.2015.10.018
29. Lansdorp BM, Tabrizi SJ, Dittmore A, Saleh OA (2013) A high-speed magnetic tweezer beyond 10,000 frames per second. Rev Sci Instrum 84(4):044301. https://doi.org/10.1063/1.4802678
30. Huhle A, Klaue D, Brutzer H, Daldrop P, Joo S, Otto O, Keyser UF, Seidel R (2015) Camera-based three-dimensional real-time particle tracking at kHz rates and Angstrom accuracy. Nat Commun 6:5885. https://doi.org/10.1038/ncomms6885
31. Vilfan ID, Lipfert J, Koster DA, Lemay SG, Dekker NH (2009) Magnetic tweezers for single-molecule experiments. In: Handbook of single-molecule biophysics, pp 371–395. https://doi.org/10.1007/978-0-387-76497-9_13
32. Lipfert J, Hao X, Dekker NH (2009) Quantitative modeling and optimization of magnetic tweezers. Biophys J 96(12):5040–5049. https://doi.org/10.1016/j.bpj.2009.03.055
33. De Vlaminck I, Henighan T, van Loenhout MT, Burnham DR, Dekker C (2012) Magnetic forces and DNA mechanics in multiplexed magnetic tweezers. PLoS One 7(8):e41432. https://doi.org/10.1371/journal.pone.0041432
34. Lipfert J, Wiggin M, Kerssemakers JWJ, Pedaci F, Dekker NH (2011) Freely orbiting magnetic tweezers to directly monitor changes in the twist of nucleic acids. Nat Commun 2. doi:Artn 439. https://doi.org/10.1038/Ncomms1450
35. Lipfert J, Kerssemakers JW, Jager T, Dekker NH (2010) Magnetic torque tweezers: measuring torsional stiffness in DNA and RecA-DNA filaments. Nat Methods 7(12):977–980
36. Kriegel F, Ermann N, Forbes R, Dulin D, Dekker NH, Lipfert J (2017) Probing the salt dependence of the torsional stiffness of DNA by multiplexed magnetic torque tweezers. Nucleic Acids Res 45(10):5920–5929. https://doi.org/10.1093/nar/gkx280
37. Otto O, Czerwinski F, Gornall JL, Stober G, Oddershede LB, Seidel R, Keyser UF (2010) Real-time particle tracking at 10,000 fps using optical fiber illumination. Opt Express 18(22):22722–22733
38. Dulin D, Barland S, Hachair X, Pedaci F (2014) Efficient illumination for microsecond tracking microscopy. PLoS One 9(9):e107335. https://doi.org/10.1371/journal.pone.0107335
39. Rieu M, Vieille T, Radou G, Jeanneret R, Ruiz-Gutierrez N, Ducos B, Allemand JF, Croquette V (2021) Parallel, linear, and sub-nanometric 3D tracking of microparticles with Stereo Darkfield Interferometry. Sci

Adv 7(6). https://doi.org/10.1126/sciadv.abe3902
40. Gosse C, Croquette V (2002) Magnetic tweezers: micromanipulation and force measurement at the molecular level. Biophys J 82(6): 3314–3329
41. Strick T (1999) Mechanical supercoiling of DNA and its relaxation by topoisomerases. Ph.D. Thesis, Paris VI, Paris
42. van Loenhout MT, Kerssemakers JW, De Vlaminck I, Dekker C (2012) Non-bias-limited tracking of spherical particles, enabling nanometer resolution at low magnification. Biophys J 102(10):2362–2371. https://doi.org/10.1016/j.bpj.2012.03.073
43. Winzor DJ, Jackson CM (2006) Interpretation of the temperature dependence of equilibrium and rate constants. J Mol Recognit 19(5):389–407. https://doi.org/10.1002/jmr.799
44. Gollnick B, Carrasco C, Zuttion F, Gilhooly NS, Dillingham MS, Moreno-Herrero F (2015) Probing DNA helicase kinetics with temperature-controlled magnetic tweezers. Small 11(11):1273–1284. https://doi.org/10.1002/smll.201402686
45. Kriegel F, Matek C, Drsata T, Kulenkampff K, Tschirpke S, Zacharias M, Lankas F, Lipfert J (2018) The temperature dependence of the helical twist of DNA. Nucleic Acids Res 46(15):7998–8009. https://doi.org/10.1093/nar/gky599
46. Seifert M, van Nies P, Papini FS, Arnold JJ, Poranen MM, Cameron CE, Depken M, Dulin D (2020) Temperature controlled high-throughput magnetic tweezers show striking difference in activation energies of replicating viral RNA-dependent RNA polymerases. Nucleic Acids Res 48(10): 5591–5602. https://doi.org/10.1093/nar/gkaa233
47. Janissen R, Berghuis BA, Dulin D, Wink M, van Laar T, Dekker NH (2014) Invincible DNA tethers: covalent DNA anchoring for enhanced temporal and force stability in magnetic tweezers experiments. Nucleic Acids Res 42(18):e137. https://doi.org/10.1093/nar/gku677
48. Eeftens JM, van der Torre J, Burnham DR, Dekker C (2015) Copper-free click chemistry for attachment of biomolecules in magnetic tweezers. BMC Biophys 8:9. https://doi.org/10.1186/s13628-015-0023-9
49. Bera SC, Seifert M, Kirchdoerfer RN, van Nies P, Wubulikasimu Y, Quack S, Papini FS, Arnold JJ, Canard B, Cameron CE, Depken M, Dulin D (2021) The nucleotide addition cycle of the SARS-CoV-2 polymerase. Cell Rep 36(9):109650. https://doi.org/10.1016/j.celrep.2021.109650
50. Bera SC, America PPB, Maatsola S, Seifert M, Ostrofet E, Cnossen J, Spermann M, Papini FS, Depken M, Malinen AM, Dulin D (2022) Quantitative parameters of bacterial RNA polymerase open-complex formation, stabilization and disruption on a consensus promoter. Nucleic Acids Res 50(13): 7511–7528. https://doi.org/10.1093/nar/gkac560
51. Papini FS, Seifert M, Dulin D (2019) High-yield fabrication of DNA and RNA constructs for single molecule force and torque spectroscopy experiments. Nucleic Acids Res 47(22): e144. https://doi.org/10.1093/nar/gkz851
52. Bell NAW, Molloy JE (2022) Efficient golden gate assembly of DNA constructs for single molecule force spectroscopy and imaging. Nucleic Acids Res 50(13):e77. https://doi.org/10.1093/nar/gkac300
53. Lu Y, Bianco P (2021) High-yield purification of exceptional-quality, single-molecule DNA substrates. J Biol Methods 8(1):e145. https://doi.org/10.14440/jbm.2021.350
54. Berghuis BA, Kober M, van Laar T, Dekker NH (2016) High-throughput, high-force probing of DNA-protein interactions with magnetic tweezers. Methods 105:90–98. https://doi.org/10.1016/j.ymeth.2016.03.025
55. Manosas M, Meglio A, Spiering MM, Ding F, Benkovic SJ, Barre FX, Saleh OA, Allemand JF, Bensimon D, Croquette V (2010) Magnetic tweezers for the study of DNA tracking motors. Methods Enzymol 475:297–320. https://doi.org/10.1016/S0076-6879(10)75013-8
56. Paik DH, Roskens VA, Perkins TT (2013) Torsionally constrained DNA for single-molecule assays: an efficient, ligation-free method. Nucleic Acids Res 41(19):e179. https://doi.org/10.1093/nar/gkt699
57. Charvin G, Allemand JF, Strick TR, Bensimon D, Croquette V (2004) Twisting DNA: single molecule studies. Contemp Phys 45(5):383–403. https://doi.org/10.1080/00107510410001697279
58. van Oene MM, Dickinson LE, Pedaci F, Kober M, Dulin D, Lipfert J, Dekker NH (2015) Biological magnetometry: torque on superparamagnetic beads in magnetic fields. Phys Rev Lett 114(21):218301. https://doi.org/10.1103/PhysRevLett.114.218301

59. Yu Z, Dulin D, Cnossen J, Kober M, van Oene MM, Ordu O, Berghuis BA, Hensgens T, Lipfert J, Dekker NH (2014) A force calibration standard for magnetic tweezers. Rev Sci Instrum 85(12):123114. https://doi.org/10.1063/1.4904148
60. te Velthuis A, Kerssemakers JWJ, Lipfert J, Dekker NH (2010) Quantitative guidelines for force calibration through spectral analysis of magnetic tweezers data. Biophys J 99(4): 1292–1302. https://doi.org/10.1016/j.bpj.2010.06.008
61. Ostrofet E, Papini FS, Dulin D (2018) Correction-free force calibration for magnetic tweezers experiments. Sci Rep 8(1):15920. https://doi.org/10.1038/s41598-018-34360-4
62. Chen H, Fu H, Zhu X, Cong P, Nakamura F, Yan J (2011) Improved high-force magnetic tweezers for stretching and refolding of proteins and short DNA. Biophys J 100(2): 517–523. https://doi.org/10.1016/j.bpj.2010.12.3700
63. Schaffer E, Norrelykke SF, Howard J (2007) Surface forces and drag coefficients of microspheres near a plane surface measured with optical tweezers. Langmuir 23(7): 3654–3665. https://doi.org/10.1021/la0622368
64. Lansdorp BM, Saleh OA (2012) Power spectrum and Allan variance methods for calibrating single-molecule video-tracking instruments. Rev Sci Instrum 83(2):025115. https://doi.org/10.1063/1.3687431
65. Morgan IL, Saleh OA (2021) Tweezepy: a python package for calibrating forces in single-molecule video-tracking experiments. PLoS One 16(12):e0262028. https://doi.org/10.1371/journal.pone.0262028
66. Daldrop P, Brutzer H, Huhle A, Kauert DJ, Seidel R (2015) Extending the range for force calibration in magnetic tweezers. Biophys J 108(10):2550–2561. https://doi.org/10.1016/j.bpj.2015.04.011
67. Shon MJ, Rah SH, Yoon TY (2019) Submicrometer elasticity of double-stranded DNA revealed by precision force-extension measurements with magnetic tweezers. Sci Adv 5(6):eaav1697. https://doi.org/10.1126/sciadv.aav1697
68. Sitters G, Kamsma D, Thalhammer G, Ritsch-Marte M, Peterman EJ, Wuite GJ (2015) Acoustic force spectroscopy. Nat Methods 12(1):47–50. https://doi.org/10.1038/nmeth.3183
69. Ostrofet E, Papini FS, Dulin D (2020) High spatiotemporal resolution data from a custom magnetic tweezers instrument. Data Brief 30: 105397. https://doi.org/10.1016/j.dib.2020.105397
70. Bustamante C, Marko JF, Siggia ED, Smith S (1994) Entropic elasticity of lambda-phage DNA. Science (New York, NY) 265(5178): 1599–1600
71. Burnham DR, De Vlaminck I, Henighan T, Dekker C (2014) Skewed brownian fluctuations in single-molecule magnetic tweezers. PLoS One 9(9):e108271. https://doi.org/10.1371/journal.pone.0108271
72. Kriegel F, Vanderlinden W, Nicolaus T, Kardinal A, Lipfert J (2018) Measuring single-molecule twist and torque in multiplexed magnetic tweezers. Methods Mol Biol 1814:75–98. https://doi.org/10.1007/978-1-4939-8591-3_6
73. Strick TR, Allemand JF, Bensimon D, Croquette V (2000) Stress-induced structural transitions in DNA and proteins. Annu Rev Biophys Biomol Struct 29:523–543. https://doi.org/10.1146/annurev.biophys.29.1.523
74. Forth S, Deufel C, Sheinin MY, Daniels B, Sethna JP, Wang MD (2008) Abrupt buckling transition observed during the plectoneme formation of individual DNA molecules. Phys Rev Lett 100(14):148301. https://doi.org/10.1103/PhysRevLett.100.148301
75. Bryant Z, Stone MD, Gore J, Smith SB, Cozzarelli NR, Bustamante C (2003) Structural transitions and elasticity from torque measurements on DNA. Nature 424(6946): 338–341. https://doi.org/10.1038/nature01810. nature01810 [pii]
76. Revyakin A, Ebright RH, Strick TR (2004) Promoter unwinding and promoter clearance by RNA polymerase: detection by single-molecule DNA nanomanipulation. Proc Natl Acad Sci U S A 101(14):4776–4780. https://doi.org/10.1073/pnas.0307241101
77. Brutzer H, Luzzietti N, Klaue D, Seidel R (2010) Energetics at the DNA supercoiling transition. Biophys J 98(7):1267–1276. https://doi.org/10.1016/j.bpj.2009.12.4292
78. Strick TR, Dessinges MN, Charvin G, Dekker NH, Allemand JF, Bensimon D, Croquette V (2003) Stretching of macromolecules and proteins. Rep Prog Phys 66(1):1–45
79. Graves ET, Duboc C, Fan J, Stransky F, Leroux-Coyau M, Strick TR (2015) A dynamic DNA-repair complex observed by correlative single-molecule nanomanipulation and fluorescence. Nat Struct Mol Biol 22(6): 452–457. https://doi.org/10.1038/nsmb.3019

80. Seol Y, Neuman KC (2018) Combined magnetic tweezers and micro-mirror total internal reflection fluorescence microscope for single-molecule manipulation and visualization. Methods Mol Biol 1665:297–316. https://doi.org/10.1007/978-1-4939-7271-5_16
81. Brutzer H, Schwarz FW, Seidel R (2012) Scanning evanescent fields using a pointlike light source and a nanomechanical DNA gear. Nano Lett 12(1):473–478. https://doi.org/10.1021/nl203876w
82. Kemmerich FE, Swoboda M, Kauert DJ, Grieb MS, Hahn S, Schwarz FW, Seidel R, Schlierf M (2016) Simultaneous single-molecule force and fluorescence sampling of DNA nanostructure conformations using magnetic tweezers. Nano Lett 16(1): 381–386. https://doi.org/10.1021/acs.nanolett.5b03956
83. van Loenhout MT, de Grunt MV, Dekker C (2012) Dynamics of DNA supercoils. Science (New York, NY) 338(6103):94–97. https://doi.org/10.1126/science.1225810
84. Schwarz FW, Toth J, van Aelst K, Cui G, Clausing S, Szczelkun MD, Seidel R (2013) The helicase-like domains of type III restriction enzymes trigger long-range diffusion along DNA. Science (New York, NY) 340(6130):353–356. https://doi.org/10.1126/science.1231122
85. Madariaga-Marcos J, Hormeno S, Pastrana CL, Fisher GLM, Dillingham MS, Moreno-Herrero F (2018) Force determination in lateral magnetic tweezers combined with TIRF microscopy. Nanoscale 10(9):4579–4590. https://doi.org/10.1039/c7nr07344e
86. Lebel P, Basu A, Oberstrass FC, Tretter EM, Bryant Z (2014) Gold rotor bead tracking for high-speed measurements of DNA twist, torque and extension. Nat Methods 11(4): 456–462. https://doi.org/10.1038/nmeth.2854
87. De Vlaminck I, van Loenhout MT, Zweifel L, den Blanken J, Hooning K, Hage S, Kerssemakers J, Dekker C (2012) Mechanism of homology recognition in DNA recombination from dual-molecule experiments. Mol Cell 46(5):616–624. https://doi.org/10.1016/j.molcel.2012.03.029
88. Bauer MS, Gruber S, Hausch A, Gomes P, Milles LF, Nicolaus T, Schendel LC, Navajas PL, Procko E, Lietha D, Melo MCR, Bernardi RC, Gaub HE, Lipfert J (2022) A tethered ligand assay to probe SARS-CoV-2:ACE2 interactions. Proc Natl Acad Sci U S A 119(14):e2114397119. https://doi.org/10.1073/pnas.2114397119
89. Wang Y, Barnett SFH, Le S, Guo Z, Zhong X, Kanchanawong P, Yan J (2019) Label-free single-molecule quantification of rapamycin-induced FKBP-FRB dimerization for direct control of cellular mechanotransduction. Nano Lett 19(10):7514–7525. https://doi.org/10.1021/acs.nanolett.9b03364
90. Seifert M, Bera SC, van Nies P, Kirchdoerfer RN, Shannon A, Le TT, Meng X, Xia H, Wood JM, Harris LD, Papini FS, Arnold JJ, Almo S, Grove TL, Shi PY, Xiang Y, Canard B, Depken M, Cameron CE, Dulin D (2021) Inhibition of SARS-CoV-2 polymerase by nucleotide analogs from a single-molecule perspective. elife 10. https://doi.org/10.7554/eLife.70968
91. Dulin D, Arnold JJ, van Laar T, Oh HS, Lee C, Perkins AL, Harki DA, Depken M, Cameron CE, Dekker NH (2017) Signatures of nucleotide analog incorporation by an RNA-dependent RNA polymerase revealed using high-throughput magnetic tweezers. Cell Rep 21(4):1063–1076. https://doi.org/10.1016/j.celrep.2017.10.005
92. Dulin D, Vilfan ID, Berghuis BA, Poranen MM, Depken M, Dekker NH (2015) Backtracking behavior in viral RNA-dependent RNA polymerase provides the basis for a second initiation site. Nucleic Acids Res 43(21): 10421–10429. https://doi.org/10.1093/nar/gkv1098
93. Janissen R, Eslami-Mossallam B, Artsimovitch I, Depken M, Dekker NH (2022) High-throughput single-molecule experiments reveal heterogeneity, state switching, and three interconnected pause states in transcription. Cell Rep 39(4): 110749. https://doi.org/10.1016/j.celrep.2022.110749
94. Hodeib S, Raj S, Manosas M, Zhang W, Bagchi D, Ducos B, Allemand JF, Bensimon D, Croquette V (2016) Single molecule studies of helicases with magnetic tweezers. Methods 105:3–15. https://doi.org/10.1016/j.ymeth.2016.06.019
95. Rieu M, Valle-Orero J, Ducos B, Allemand JF, Croquette V (2021) Single-molecule kinetic locking allows fluorescence-free quantification of protein/nucleic-acid binding. Commun Biol 4(1):1083. https://doi.org/10.1038/s42003-021-02606-z
96. Burnham DR, Kose HB, Hoyle RB, Yardimci H (2019) The mechanism of DNA unwinding by the eukaryotic replicative helicase. Nat Commun 10(1):2159. https://doi.org/10.1038/s41467-019-09896-2
97. Seol Y, Harami GM, Kovacs M, Neuman KC (2019) Homology sensing via non-linear

amplification of sequence-dependent pausing by RecQ helicase. elife 8. https://doi.org/10.7554/eLife.45909

98. Mills M, Harami GM, Seol Y, Gyimesi M, Martina M, Kovacs ZJ, Kovacs M, Neuman KC (2017) RecQ helicase triggers a binding mode change in the SSB-DNA complex to efficiently initiate DNA unwinding. Nucleic Acids Res 45(20):11878–11890. https://doi.org/10.1093/nar/gkx939
99. Klaue D, Kobbe D, Kemmerich F, Kozikowska A, Puchta H, Seidel R (2013) Fork sensing and strand switching control antagonistic activities of RecQ helicases. Nat Commun 4:2024. https://doi.org/10.1038/ncomms3024
100. Lionnet T, Spiering MM, Benkovic SJ, Bensimon D, Croquette V (2007) Real-time observation of bacteriophage T4 gp41 helicase reveals an unwinding mechanism. Proc Natl Acad Sci U S A 104(50):19790–19795. https://doi.org/10.1073/pnas.0709793104. 0709793104 [pii]
101. Dessinges MN, Lionnet T, Xi XG, Bensimon D, Croquette V (2004) Single-molecule assay reveals strand switching and enhanced processivity of UvrD. Proc Natl Acad Sci U S A 101(17):6439–6444. https://doi.org/10.1073/pnas.0306713101. 0306713101 [pii]
102. Manosas M, Xi XG, Bensimon D, Croquette V (2010) Active and passive mechanisms of helicases. Nucleic Acids Res 38(16):5518–5526. https://doi.org/10.1093/nar/gkq273
103. Fiorini F, Bagchi D, Le Hir H, Croquette V (2015) Human Upf1 is a highly processive RNA helicase and translocase with RNP remodelling activities. Nat Commun 6:7581. https://doi.org/10.1038/ncomms8581
104. Bagchi D, Manosas M, Zhang W, Manthei KA, Hodeib S, Ducos B, Keck JL, Croquette V (2018) Single molecule kinetics uncover roles for E. coli RecQ DNA helicase domains and interaction with SSB. Nucleic Acids Res 46(16):8500–8515. https://doi.org/10.1093/nar/gky647
105. Eeftens JM, Bisht S, Kerssemakers J, Kschonsak M, Haering CH, Dekker C (2017) Real-time detection of condensin-driven DNA compaction reveals a multistep binding mechanism. EMBO J 36(23):3448–3457. https://doi.org/10.15252/embj.201797596
106. Elbatsh AMO, Kim E, Eeftens JM, Raaijmakers JA, van der Weide RH, Garcia-Nieto A, Bravo S, Ganji M, Uit de Bos J, Teunissen H, Medema RH, de Wit E, Haering CH, Dekker C, Rowland BD (2019) Distinct roles for condensin's two ATPase sites in chromosome condensation. Mol Cell 76(5):724–737. e725. https://doi.org/10.1016/j.molcel.2019.09.020
107. van der Heijden T, Seidel R, Modesti M, Kanaar R, Wyman C, Dekker C (2007) Real-time assembly and disassembly of human RAD51 filaments on individual DNA molecules. Nucleic Acids Res 35(17):5646–5657. https://doi.org/10.1093/nar/gkm629
108. Liu Y, Chen H, Kenney LJ, Yan J (2010) A divalent switch drives H-NS/DNA-binding conformations between stiffening and bridging modes. Genes Dev 24(4):339–344. https://doi.org/10.1101/gad.1883510
109. Gulvady R, Gao Y, Kenney LJ, Yan J (2018) A single molecule analysis of H-NS uncouples DNA binding affinity from DNA specificity. Nucleic Acids Res 46(19):10216–10224. https://doi.org/10.1093/nar/gky826
110. Fu H, Le S, Muniyappa K, Yan J (2013) Dynamics and regulation of RecA polymerization and de-polymerization on double-stranded DNA. PLoS One 8(6):e66712. https://doi.org/10.1371/journal.pone.0066712
111. Vtyurina NN, Dulin D, Docter MW, Meyer AS, Dekker NH, Abbondanzieri EA (2016) Hysteresis in DNA compaction by Dps is described by an Ising model. Proc Natl Acad Sci U S A 113(18):4982–4987. https://doi.org/10.1073/pnas.1521241113
112. Bell NAW, Haynes PJ, Brunner K, de Oliveira TM, Flocco MM, Hoogenboom BW, Molloy JE (2021) Single-molecule measurements reveal that PARP1 condenses DNA by loop stabilization. Sci Adv 7(33). https://doi.org/10.1126/sciadv.abf3641
113. Meng H, Andresen K, van Noort J (2015) Quantitative analysis of single-molecule force spectroscopy on folded chromatin fibers. Nucleic Acids Res 43(7):3578–3590. https://doi.org/10.1093/nar/gkv215
114. Kruithof M, Chien FT, Routh A, Logie C, Rhodes D, van Noort J (2009) Single-molecule force spectroscopy reveals a highly compliant helical folding for the 30-nm chromatin fiber. Nat Struct Mol Biol 16(5):534–540. https://doi.org/10.1038/nsmb.1590
115. Kruithof M, Chien F, de Jager M, van Noort J (2008) Subpiconewton dynamic force spectroscopy using magnetic tweezers. Biophys J 94(6):2343–2348. biophysj.107.121673 [pii]. https://doi.org/10.1529/biophysj.107.121673

116. Bancaud A, Conde e Silva N, Barbi M, Wagner G, Allemand JF, Mozziconacci J, Lavelle C, Croquette V, Victor JM, Prunell A, Viovy JL (2006) Structural plasticity of single chromatin fibers revealed by torsional manipulation. Nat Struct Mol Biol 13(5):444–450. https://doi.org/10.1038/nsmb1087. doi:nsmb1087 [pii]
117. Simon M, North JA, Shimko JC, Forties RA, Ferdinand MB, Manohar M, Zhang M, Fishel R, Ottesen JJ, Poirier MG (2011) Histone fold modifications control nucleosome unwrapping and disassembly. Proc Natl Acad Sci U S A 108(31):12711–12716. https://doi.org/10.1073/pnas.1106264108
118. Koster DA, Crut A, Shuman S, Bjornsti MA, Dekker NH (2010) Cellular strategies for regulating DNA supercoiling: a single-molecule perspective. Cell 142(4):519–530. https://doi.org/10.1016/j.cell.2010.08.001. S0092-8674(10)00896-2 [pii]
119. Lipfert J, Koster DA, Vilfan ID, Hage S, Dekker NH (2009) Single-molecule magnetic tweezers studies of type IB topoisomerases. DNA Topoisomerases: Methods and Protocols 582:71–89. https://doi.org/10.1007/978-1-60761-340-4_7
120. Mills M, Tse-Dinh YC, Neuman KC (2018) Direct observation of topoisomerase IA gate dynamics. Nat Struct Mol Biol 25(12):1111–1118. https://doi.org/10.1038/s41594-018-0158-x
121. McKie SJ, Desai PR, Seol Y, Allen AM, Maxwell A, Neuman KC (2022) Topoisomerase VI is a chirally-selective, preferential DNA decatenase. elife 11. https://doi.org/10.7554/eLife.67021
122. Strick TR, Croquette V, Bensimon D (2000) Single-molecule analysis of DNA uncoiling by a type II topoisomerase. Nature 404(6780):901–904. https://doi.org/10.1038/35009144
123. Koster DA, Palle K, Bot ES, Bjornsti MA, Dekker NH (2007) Antitumour drugs impede DNA uncoiling by topoisomerase I. Nature 448(7150):213–217. https://doi.org/10.1038/nature05938
124. Koster DA, Croquette V, Dekker C, Shuman S, Dekker NH (2005) Friction and torque govern the relaxation of DNA supercoils by eukaryotic topoisomerase IB. Nature 434(7033):671–674. https://doi.org/10.1038/nature03395
125. Revyakin A, Liu C, Ebright RH, Strick TR (2006) Abortive initiation and productive initiation by RNA polymerase involve DNA scrunching. Science (New York, NY) 314(5802):1139–1143. https://doi.org/10.1126/science.1131398
126. Tomko EJ, Fishburn J, Hahn S, Galburt EA (2017) TFIIH generates a six-base-pair open complex during RNAP II transcription initiation and start-site scanning. Nat Struct Mol Biol 24(12):1139–1145. https://doi.org/10.1038/nsmb.3500
127. Lerner E, Chung S, Allen BL, Wang S, Lee J, Lu SW, Grimaud LW, Ingargiola A, Michalet X, Alhadid Y, Borukhov S, Strick TR, Taatjes DJ, Weiss S (2016) Backtracked and paused transcription initiation intermediate of Escherichia coli RNA polymerase. Proc Natl Acad Sci U S A 113(43):E6562–E6571. https://doi.org/10.1073/pnas.1605038113
128. Yu LB, Winkelman JT, Pukhrambam C, Strick TR, Nickels BE, Ebright RH (2017) The mechanism of variability in transcription start site selection. elife 6. ARTN e32038. https://doi.org/10.7554/eLife.32038
129. Portman JR, Brouwer GM, Bollins J, Savery NJ, Strick TR (2021) Cotranscriptional R-loop formation by Mfd involves topological partitioning of DNA. Proc Natl Acad Sci U S A 118(15). https://doi.org/10.1073/pnas.2019630118
130. Szczelkun MD, Tikhomirova MS, Sinkunas T, Gasiunas G, Karvelis T, Pschera P, Siksnys V, Seidel R (2014) Direct observation of R-loop formation by single RNA-guided Cas9 and Cascade effector complexes. Proc Natl Acad Sci U S A 111(27):9798–9803. https://doi.org/10.1073/pnas.1402597111
131. Rutkauskas M, Sinkunas T, Songailiene I, Tikhomirova MS, Siksnys V, Seidel R (2015) Directional R-loop formation by the CRISPR-Cas surveillance complex cascade provides efficient off-target site rejection. Cell Rep. https://doi.org/10.1016/j.celrep.2015.01.067
132. Kaczmarczyk A, Meng H, Ordu O, Noort JV, Dekker NH (2020) Chromatin fibers stabilize nucleosomes under torsional stress. Nat Commun 11(1):126. https://doi.org/10.1038/s41467-019-13891-y
133. Henneman B, Brouwer TB, Erkelens AM, Kuijntjes GJ, van Emmerik C, van der Valk RA, Timmer M, Kirolos NCS, van Ingen H, van Noort J, Dame RT (2021) Mechanical and structural properties of archaeal hypernucleosomes. Nucleic Acids Res 49(8):4338–4349. https://doi.org/10.1093/nar/gkaa1196
134. Vlijm R, Lee M, Lipfert J, Lusser A, Dekker C, Dekker NH (2015) Nucleosome

assembly dynamics involve spontaneous fluctuations in the handedness of tetrasomes. Cell Rep 10(2):216–225. https://doi.org/10.1016/j.celrep.2014.12.022

135. Vlijm R, Kim SH, De Zwart PL, Dalal Y, Dekker C (2017) The supercoiling state of DNA determines the handedness of both H3 and CENP-A nucleosomes. Nanoscale 9(5):1862–1870. https://doi.org/10.1039/c6nr06245h
136. Ordu O, Kremser L, Lusser A, Dekker NH (2018) Modification of the histone tetramer at the H3-H3 interface impacts tetrasome conformations and dynamics. J Chem Phys 148(12):123323. https://doi.org/10.1063/1.5009100
137. Lee M, Lipfert J, Sanchez H, Wyman C, Dekker NH (2013) Structural and torsional properties of the RAD51-dsDNA nucleoprotein filament. Nucleic Acids Res 41(14):7023–7030. https://doi.org/10.1093/nar/gkt425
138. Fulconis R, Bancaud A, Allemand JF, Croquette V, Dutreix M, Viovy JL (2004) Twisting and untwisting a single DNA molecule covered by RecA protein. Biophys J 87(4):2552–2563. https://doi.org/10.1529/biophysj.104.043059
139. Atwell S, Disseau L, Stasiak AZ, Stasiak A, Renodon-Corniere A, Takahashi M, Viovy JL, Cappello G (2012) Probing Rad51-DNA interactions by changing DNA twist. Nucleic Acids Res 40(22):11769–11776. https://doi.org/10.1093/nar/gks1131
140. Arata H, Dupont A, Mine-Hattab J, Disseau L, Renodon-Corniere A, Takahashi M, Viovy JL, Cappello G (2009) Direct observation of twisting steps during Rad51 polymerization on DNA. Proc Natl Acad Sci U S A 106(46):19239–19244. https://doi.org/10.1073/pnas.0902234106. 0902234106 [pii]
141. Lim CJ, Kenney LJ, Yan J (2014) Single-molecule studies on the mechanical interplay between DNA supercoiling and H-NS DNA architectural properties. Nucleic Acids Res 42(13):8369–8378. https://doi.org/10.1093/nar/gku566